Sensors and Actuators A 247 (2016) 379–388

Contents lists available at ScienceDirect

Sensors and Actuators A: Physical

journal homepage: www.elsevier.com/locate/sna

Complete electromechanical analysis of electrostatic kinetic energy harvesters biased with a continuous conditioning circuit

Eoghan O'Riordan [a,*], Dimitri Galayko [b], Philippe Basset [c], Elena Blokhina [a]

[a] University College Dublin, Ireland
[b] LIP6, UPMC, Paris, France
[c] Université Paris-Est, ESYCOM, ESIEE Paris, Noisy-Le-Grand, France

ARTICLE INFO

Article history:
Received 19 January 2016
Received in revised form 2 May 2016
Accepted 13 June 2016
Available online 16 June 2016

Keywords:
Electromechanical effects
Electrostatic kinetic energy harvester
MEMS energy harvesters
Energy conversion

ABSTRACT

This paper presents a comprehensive electromechanical study of an electrostatic kinetic energy harvester (eKEH) biased with a continuous voltage. This simple circuit refers to any capacitive transducer with an in-built voltage source, such as an electret, or DC biased transducer connected directly to a resistive load. It is commonly used for the characterisation of experimental transducers. However there is a void of any unified discussion focusing on the circuits influence on the transducer, due to electromechanical coupling in the transducer. The electromechanical coupling causes numerous nonlinear effects, any of which can result in inconsistent results and disjointed conclusions of experimental devices. This article seeks to present analytic tools which can be employed for systems of this type and discusses some of the results obtained from these techniques. Along with analysis and characterisation of the circuit dynamics, the results are compared with an experimental device and presented in terms of design of the system and conclusions drawn relating to the optimum operation point.

1. Introduction

Throughout the last decade, small scale mechanically driven electricity generators have continued to receive increasing attention as autonomous power sources for low power electronic devices. Mechanical energy harvesting devices are generally referred to as kinetic energy harvesters (KEH). Electrostatic kinetic energy harvesters (eKEH) convert kinetic energy of the environment into electrical energy using a capacitive transducer. EKEH are particularly suitable for microscale implementation due to the ease with which they can be incorporated into existing MEMS fabrication technologies [1–4].

The structure of eKEHs includes a mechanical part, an electrical component and a capacitive transducer interfacing them. The mechanical part and the transducer are usually implemented as a single miniature device. Many authors have made novel advances in the area of eKEH with different geometries of the mechanical part and of the transducer: dual cavity MEMS resonators [5], 3 degree of freedom MEMS transducers [6,7], multi-layer comb geometries [8] and devices employing mechanical impacts [9]. The goal of these devices is to obtain the largest possible time variation of the transducer capacitance when the device is submitted to external vibrations.

A capacitive transducer requires a biasing in order to generate electrical energy, achieved by the electrical conditioning electronics. In comparison with the mechanically elaborate MEMS for eKEH, there has been much less attention given to the problem of the conditioning electronics. Most MEMS eKEH devices are characterised using a resistive load and continuous voltage source, called the "continuous conditioning circuit", whose topology is presented in Fig. 1. The continuous conditioning circuit was first discussed in [10,11]. It was proposed as an electric interface between a resistive load and a capacitive transducer with an electret layer: this is a charged dielectric layer biasing the capacitor plates [12]. Indeed, a large pre-charged capacitor C_{res} or a DC voltage source in series with a variable capacitor C_t represents, exactly, a lumped model of a capacitive transducer biased by an electret (Fig. 1b). The name of the circuit comes from the fact that all voltages and currents of the circuit are continuous functions of time, which is not true for more sophisticated circuits that use switches or diodes [2,13–15].

In spite of the frequent use of this circuit, to the best knowledge of the authors, there has been no complete study of the system from the perspective of the designer, presented in the literature. The three following basic questions are still not fully answered:

* Corresponding author. Tel.: +353 17161913.
E-mail address: eoghan.o-riordan@ucdconnect.ie (E. O'Riordan).

http://dx.doi.org/10.1016/j.sna.2016.06.018
0924-4247/

Nomenclature

x	mobile mass displacement
q	instantaneous charge on transducer
$C_t(x)$	transducer capacitance characteristic
f_t	transducer force
A_{ext}	acceleration amplitude of external vibrations
ω_{ext}	frequency of external vibrations
d	approximated gap between fingers
C_0	transducer capacitance at rest
R_L	resistive load
τ	normalised time
y	normalised displacement
Q	normalised charge
a_0	normalised steady-state resonator displacement
F_t	normalised transducer force
β	normalised dissipation
Ω	normalised external driving frequency
α	normalised external acceleration amplitude
σ	normalised frequency mismatch
Ψ	mechanical impedance
$\dot{F}$	phasor of sinusoidal force
$\dot{U}$	phasor of velocity

(i) *Optimal load resistance and converted power*. Given the parameters of the capacitance C_t variation and the bias voltage V_0, what value of the load resistance yields a maximal dissipated (converted) power and what is the corresponding converted power?

(ii) *Electromechanical coupling*. The last two questions are asked under the simplified hypothesis of a known and fixed transducer capacitance variation. In the case when there is electromechanical coupling, the underlying question is: how does the conditioning circuit impact on the resonator of the MEMS device used in the harvester, and in turn affect the optimum parameter and converted power.

(iii) *Resonance frequency shift*. It is known that a mechanical resonator experiences a modification of its resonance frequency, when interfaced with a capacitive transducer biased by a voltage source [16]. This phenomenon is well studied and described in the literature. However, the same system biased with a voltage source *in series with a resistance as in Fig. 1a* highlights a *different* resonance frequency shift, which may go from zero to the value observed in a configuration with a single voltage source. No quantitative characterisation of this phenomenon in the continuous conditioning circuit has been presented to date.

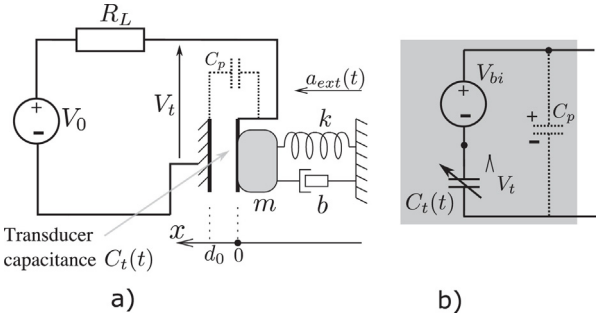

Fig. 1. (a) Block diagram of the continuous conditioning circuit. In this study the continuous circuit represents all circuit configurations which employ a capacitive transducer, resistive load and some internal or external voltage to provide the initial bias on the transducer. (b) Equivalent schematic of a capacitive transducer biased by an electret layer.

There are few responses to these questions even in the case of very simple configurations, e.g., a linear resonator, sinusoidal external vibrations, and a transducer with a simple characteristic "capacitance-displacement". However, many modern studies on KEH focus on nonlinear mechanical subsystems, considering the nonlinearity as a tool for widening the frequency response [17–19]. Also, many works use sophisticated capacitive transducers (symmetrical gap closing, saw-tooth, etc.). When such devices are inserted into the continuous conditioning circuit, no existing tool offers an insight into the dynamics of the whole system, and, excluding numerical simulation, no method predicts its operational performances. Such voids existing in the comprehension of very frequently used configurations are explained by a high mathematical complexity in the analysis of the circuit. Indeed, even in the case when only the electrical domain is considered, the circuit is described by a linear equation with variable coefficients, which is not integrable in closed form.

While not abundant, tools for analysing systems of this type exist in the literature [20–22]. This article presents a fundamental study of the coupled electromechanical behaviour of an eKEH employing a continuous conditioning circuit. The originality of the study is twofold. First, an insight is proposed into phenomena which have never been discussed before: (i) the relationship existing between the resonance frequency shift and the value of the load resistance, (ii) the influence of the capacity-displacement function of the transducer on the system dynamics. Secondly, we propose a set of analytical and semi-analytical tools allowing a rapid assessment of the circuit performance as a function of the system parameters, without performing time consuming simulations which provide only particular results.

Section 2 presents the electrical and mechanical models describing the system, shown in Fig. 1. Semi-analytic methods are employed for analysis and design in Sections 3 and 4. Finally, results from the different semi-analytic electromechanical models are compared with the experimental device in Section 5.

2. Statement of the problem

2.1. Primary electromechanical model

A high quality (high-Q) mechanical resonator, driven by ambient vibrations, causes a variation in the capacitance, C_t, of the variable transducer. The resonator frame moves due to the external vibrations. The displacement x of the mobile mass with respect to the frame is also affected by the transducer force f_t.

$$\ddot{x} + \left(\frac{b}{m}\right)\dot{x} + \omega_0^2 x = A_{ext}\cos(\omega_{ext}t + \vartheta_0) + \frac{f_t}{m} \quad (1)$$

where m is the mass of the resonator, b is the damping coefficient, $\omega_0 = \sqrt{k/m}$ is the natural frequency, k is the spring constant, A_{ext} is the acceleration amplitude of external vibrations, ω_{ext} is the external frequency and ϑ_0 is the initial phase of the external vibrations. The quality factor is estimated from experiments. The system can be considered high-Q as it is underdamped. Typically a quality factor greater than 5 would be considered high.

The actual model of a harvester is composed of electrical and mechanical models connected through the equations of coupling. These equations come from the physics of the transducer. For the capacitive transducer, the transducer force f_t can be expressed as a

Table 1
Dimensional and dimensionless parameters.

Transducer	AO	GC	SGC
$C_t(x)$	$C_0 + x\delta$	$\frac{C_0}{1-(x/d)}$	$\frac{2C_0}{1-(x/d)^2}$
$\mathcal{C}_{tran}(y)$	$(1+y)$	$\frac{1}{1-y}$	$\frac{2}{1-y^2}$
f_t	$\frac{V_t^2}{2}\delta$	$\frac{V_t^2}{2}\frac{C_0 d}{(d-x)^2}$	$\frac{V_t^2}{2}\frac{4C_0 d^2 x}{\left(d^2-x^2\right)^2}$
F_t	$\frac{\nu_{AO}Q^2}{(y+1)^2}$	$\nu_{GC}Q^2$	$\nu_{SGC}Q^2 y$
ν_t	$\frac{V_0^2\delta^2}{2mC_0^3\omega_0^4R_L^2}$	$\frac{V_0^2}{2mC_0\omega_0^4d^2R_L^2}$	$\frac{V_0^2}{2mC_0\omega_0^4d^2R_L^2}$

function of the charge on the transducer (q) and the mobile mass position (x):

$$f_t(x, V_t) = \frac{1}{2}\frac{q^2}{C_t^2(x)}\frac{dC_t(x)}{dx} \tag{2}$$

where $C_t(x)$ is the capacitance-displacement characteristic of the transducer given by the chosen transducer geometry and dC_t/dx is a known function of the displacement, x. The force f_t expresses the influence of the electrical behaviour on the system in the mechanical domain.

The governing equations describing the electrical behaviour of the simple conditioning circuit are given by Kirchhoff's voltage law and the element equations:

$$R_L\frac{dq}{dt} + \frac{q}{C_t(x)} = V_0, \tag{3}$$

where q is the instantaneous charge on the transducer, R_L is the resistive load and $C_t(t)$ is the time evolution law of the transducer's capacitance.

In the electrical analysis, it is assumed that the evolution of C_t is defined and is independent of the dynamics of the electrical process. It is only defined by the time variation of the transducer geometry. In the electrical domain, ultimate validation of the analytical methods describing the circuit can be realised using a Spice simulator (e.g., Eldo, Hspice, Pspice, etc.), whose libraries include a macro model of a variable capacitor.

The function $C_t(x)$ is an important characteristic of the system. The three most common transducer configurations, namely the area-overlap transducer (AO), the gap-closing transducer (GC) [23] and the symmetrical gap-closing (SGC) transducer, can be modeled using the methods in this article. The capacitance-displacement characteristic for each configuration is detailed in Table 1, where C_0 is the capacitance value at rest when the displacement of the movable electrode is zero, d is the rest gap for the gap-closing transducer and δ is a characteristic coefficient of the area-overlap transducer.

2.2. Normalised model

In order to reduce the number of parameters of the complete electromechanical model and outline only essential ones, a standard normalisation is applied to Eqs. (1)–(3) [24]. We introduce the following normalised variables: time $\tau = \omega_0 t + \vartheta_0$, dissipation $\beta = b/(2m\omega_0)$, normalised external vibration frequency $\Omega = \omega_{ext}/\omega_0$, normalised charge $Q = q/Q_0$ where $Q_0 = V_0/(\omega_0 R_L)$, and the coefficient $\rho = (C_0\omega_0 R_L)^{-1}$. We also will introduce a normalisation parameter ξ (that will be different for each particular geometry) such that $y = x/\xi$ is the dimensionless displacement. The term ξ is simply $\xi = d$ for the gap closing and symmetrical gap closing transducers, and $\xi = C_0/\delta$ for the area overlap transducer. Thus, the normalised model of the system is:

$$y'' + 2\beta y' + y = \alpha\cos(\Omega\tau) + \nu_t F_t(y, Q) \tag{4a}$$

$$Q' = 1 - \rho Q\mathcal{C}_{tran}^{-1} \tag{4b}$$

where the dimensionless external acceleration amplitude is $\alpha = A_{ext}/(\omega_0^2\xi)$ and we symbolically denote $\mathcal{C}_{tran}$ as a dimensionless function describing the capacitance-displacement characteristic. Table 1 includes the dimensionless capacitance-displacement characteristic ($\mathcal{C}_{tran}(y(\tau)) \equiv \mathcal{C}_{tran}(\tau)$) and corresponding transducer forces for both dimensional (f_t) and normalised descriptions (F_t), where ν_t denotes the dimensionless coefficient of F_t.

2.3. Accounting for parasitic capacitance

Parasitic capacitance, for the transducer in Fig. 1(a), is easily incorporated into the electrical model (3) and transducer force.

$$R_L\frac{dq}{dt} + \frac{q}{C_p + C_t(x)} = V_0 \tag{5}$$

The analysis of this circuit is also applicable to electret devices. The effect of the parasitic capacitance is different for electret devices, as the parasitic capacitance is across the terminal including the transducer and bias, Fig. 1(b).

$$R_L\frac{dq}{dt}\left(1 + \frac{C_p}{C_t(x)}\right) + \frac{q}{C_t(x)} = V_0. \tag{6}$$

Note that (6) is the fusion of a system of differential equations describing the network in Fig. 1(b). It can be shown, by a linear transformation, that (5) and (6) are equivalent. The device presented in this article does not include an electret. Thus while the intention of this study is not the description of an electret device, the analysis and results of electromechanical coupling are common to both configurations of the continuous circuit.

3. Coupled analysis of the system using multiple scales

This section describes and employs a perturbation technique to acquire greater insight into the electromechanical coupling, present in all eKEH.

3.1. Analysis in the electrical domain

Before considering the analysis of the full system, we propose to present a brief analysis of the circuit in the electrical domain. It is shown that considerable difficulties arise for the fully analytical description of this simple circuit even when the electromechanical coupling is not considered.

Lets suppose that $\mathcal{C}_{tran}(\tau)$ is a known function. In this case, Eq. (4b) is a linear nonhomogeneous equation with variable coefficient whose general solution is found using a standard method [25]:

$$Q(\tau) = Q_0\, e^{-\int_0^\tau \rho\mathcal{C}_{tran}(t)^{-1}dt} + + e^{-\int_0^\tau \rho\mathcal{C}_{tran}(t)^{-1}dt} \cdot \int_0^\tau e^{\int_0^t \rho\mathcal{C}_{tran}(t_1)^{-1}dt_1}dt \tag{7}$$

Now consider a realistic form of the $\mathcal{C}_{tran}(\tau)$ function. The case detailed in this article is for the symmetrical gap closing transducer which is the configuration of the experimental transducer [26]. If the motion of the mobile mass is sinusoidal with normalised amplitude a, from Table 1 (for $\mathcal{C}_{tran}(y(\tau))$ for SGC), we obtain:

$$\mathcal{C}_{tran,SGC} = \frac{2}{1-(a\cos(\tau))^2}. \tag{8}$$

Note that $\mathcal{C}_{\text{tran}}(y(\tau))$ is not sinusoidal, even if the mobile mass vibrations are.

It can be seen that the integral (7) with (8) cannot be expressed in closed form. However, since the system is submitted to periodic parametric excitation, it is expected that all dynamic quantities are periodic in the steady-state mode. So, using the property that the function is periodic, the steady-state-solution of Q, denoted Q_{ss}, can be expressed through a Fourier Series.

$$Q_{ss}(\tau) = \mathcal{A}_0 + \sum_{n=1}^{\infty} \mathcal{A}_n \cos(nt) + \sum_{n=1}^{\infty} \mathcal{B}_n \sin(nt) \tag{9}$$

where the dc component $\mathcal{A}_0$ is equal to $I_0((\rho a^2)/(4))$, and $\mathcal{A}_n$ and $\mathcal{B}_n$ are modified Bessel functions. This formula provides an accurate model of the evolution in the electrical domain as a function of the resonator displacement. Due to the symmetry of the device, all odd members of the sum are zero, as well as $\mathcal{A}_2$ and $\mathcal{B}_4$. Hence, in most cases, truncation of the series after the fourth term ($n = 4$) provides enough precision, although under some conditions more terms would be required.

The lack of a closed form solution of (4b) presenting the electrical domain, and the complexity of the solution of (7), highlights the difficulties involved in analysing the system. On the other hand, when combined with semi-analytic techniques, such as the multiple scales method (presented later), the system of differential equations, (4a) and (4b), can be solved as a nonlinear equation while still including the nonlinear electromechanical coupling. Compared with numerical simulations, solutions of this form are significantly faster, allow further validation of the numerical solutions and allow designers gain increased insight into the system dynamics.

3.2. Multiple scales method

The method of multiple scales (MSM) was adapted in [22] to solve resonators with a capacitive interface. The multiple scales method approaches the eKEH as a simple resonator with a perturbation term. It then solves this by introducing different time scales.

A requirement of the presented method is that the transducer force F_t be periodic. This allows the transducer force be represented by a Fourier series. It is also advantageous that the system be high-Q, which is the case for narrow band energy harvesters (cf. Section 2). Further justification of the validity of the MSM for the analysis of eKEH is provided in [22]. The resulting equation provides a solution for the steady-state amplitude of oscillations, a_0, as a function of the Fourier series coefficients ($a_1(a_0)$ and $b_1(a_0)$) of $F_t(y, Q)$ and the dimensionless parameters:

$$\frac{\alpha^2}{4} = \left(a_0\sigma + \frac{\nu_t a_1(a_0)}{2}\right)^2 + \left(\beta a_0 + \frac{\nu_t b_1(a_0)}{2}\right)^2 \tag{10}$$

where σ is the dimensionless frequency mismatch ($\omega_{\text{ext}}/\omega_0 - 1$) and the Fourier coefficients are functions of the specific conditioning circuit and transducer configuration. Solving (10) for a_0, the steady-state solution of y can be determined in the form

$$y_0(\tau) = y_{\text{av},0} + a_0 \cos((1+\sigma)\tau + \theta_0 - \psi_0) \tag{11}$$

where a_0, $y_{av,0}$ and ψ_0 are the steady-state amplitude, average displacement (constant shift) and phase of oscillations. The index '0' is used to emphasize that this is a steady-state solution. As explained in [22], this approach provides information about transient dynamics of the system, and allows one to explore the dynamics around multiple stable points and identify different possible stable modes.

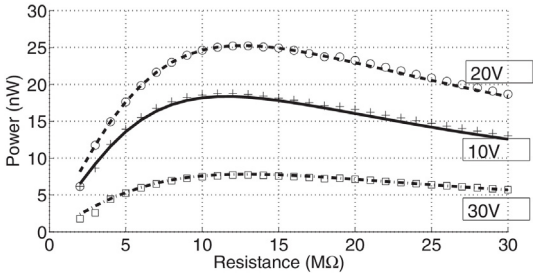

Fig. 2. Harvested power versus load resistance for various bias voltages. Lines denote solutions of the MSM and characters present solutions of the system of ordinary differential equations (1)–(3). There is an optimum resistance for the continuous circuit, roughly 11 MΩ in the presented case, for a given external excitation.

3.3. Application of the MSM analysis

It is difficult to create accurate models of nonlinear systems, as there are uncertainties in both experimental measurements and dynamic behaviour such as nonlinear damping. Thus if only one model is employed, inaccuracies of the model/measurements may not be clear. Added to this, the nonlinear equations describing eKEH cannot be solved in a closed form and therefore insights into optimal operating conditions are difficult to achieve. Accordingly there are multiple benefits to employing both numerical and semi-analytical models to achieve a greater understanding of the device behaviour. Employing semi-analytical techniques provides a greater understanding of the device dynamics. While not in a closed form, some mathematical relationships optimising the system are presented in this section.

3.3.1. Converted power

An immediate design benefit of the method is the ability to calculate the harvested power across a plane of possible design parameters. The harvested power can be calculated as the time average of the square of the current, through the resistive load, given by the equation:

$$P = \frac{R_L}{T} \int_0^T \dot{q}^2 dt \tag{12}$$

where T is the period of the resonator oscillations.

Fig. 2 shows the power for different initial biasing as a function of the load resistance (R_L). The MSM solution of (10) compared with the numerical system of Eqs. (1)–(3) shows very good accuracy. Fig. 2 not only highlights the existence of an optimum R_L, the presence of an optimum set (R_L, V_0) is also indicated.

3.3.2. Resonance frequency shift

One effect of the electromechanical coupling is electrostatic frequency modification, which affects the resonance frequency of oscillations in the resonator. Electrostatic frequency modification is the alteration of the effective stiffness of the resonator due to the interface with the conditioning circuit. This effect on the resonator displacement and velocity is shown in Fig. 3. Note this is not individually due to the conditioning circuit but also due to the capacitor geometry. An equation can be derived from (10) which describes the resonance frequency shift of the oscillations, given by:

$$\sigma_{\text{resonance shift}} = -\frac{a_1(a_0)}{2a_0} \tag{13}$$

Even in cases when the MSM approach is not as accurate, Eq. (13) provides a very good indication of the magnitude of the shift in oscillations [27]. Eq. (13) highlights the dependence of the resonance frequency shift on the first Fourier cosine term of the transducer force, and as this term is nonzero we will have a

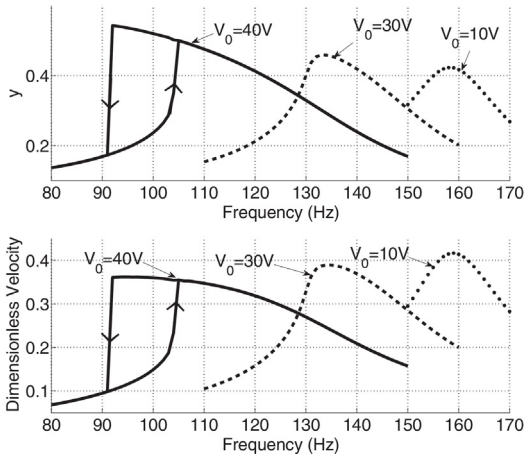

Fig. 3. The resonant frequency shift, of the mass, due to electromechanical coupling. (a) Describes the normalised displacement of the oscillating mass and (b) presents the change in the normalised velocity for the same electromechanical coupling.

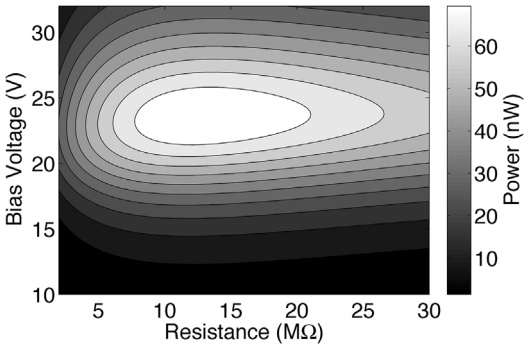

Fig. 4. Global power maximum on a plane of R_L and V_0, for fixed external vibrations (A_{ext} = 0.25 g and f_{ext} = 150 Hz). For the given external driving, the optimum is located at R_L = 13 MΩ and V_0 = 23.5 V. It changes for different external excitations, limited only by the mechanical stoppers and pull-in between the capacitor plates.

frequency shift for different system parameters. For example, in the case of the constant charge conditioning circuit presented in [22], with a gap closing transducer, $a_1(a_0) = 0$ and oscillations do not experience a shift in the resonance frequency.

3.3.3. Impact of the biasing on the displacement amplitude

According to Fig. 3(a), the amplitude of vibrations near resonance *increases* as the bias voltage increases. This seems counter-intuitive as, generally, an understanding of electromechanical coupling in eKEH would lead one to expect a decrease in the resonator oscillations for an increase in the initial bias voltage, due to the electromechanical coupling becoming stronger. However this evolution, in Fig. 3(a), is a joint effect of the increase in damping and the shift of the resonance frequency. Let us consider a linear oscillator composed of a mass, spring and damper, submitted to a sinusoidal force with amplitude F_0 at the resonance frequency ω_{res}. A simple analysis gives the amplitude of velocity and displacement U_0 and X_0, respectively:

$$U_0 = \frac{F_0}{\mu}, \quad X_0 = \frac{U_0}{\omega_{res}} = \frac{F_0}{\mu\omega_{res}} \tag{14}$$

Such a linear resonator can be considered as an equivalent linearised model of the studied KEH, where μ is a total damping accounting for the intrinsic resonator damping and for the electrostatic damping.

From the last equation it can be seen that as the damping μ increases, the velocity decreases. Indeed, for our system, from Fig. 3(b) the velocity at the resonance frequency clearly decreases as the electromechanical coupling (and thus the total damping) increases. However, the displacement amplitude X_0 is inversely proportional to the product $\omega_{res}\mu$. In our case, as the bias voltage increases, the total damping μ increases, but the resonance frequency ω_{res} decreases. As a consequence, the trend for the amplitude of displacement at the resonance is not obvious and can only be given by an analysis of the particular configuration.

Note the existence of hysteresis in Fig. 3 at 40 V, corresponding to bi-modality in the resonator displacement. The occurrence of more than one stable solution of the system is caused by the nonlinear electromechanical coupling. The Method of Multiple Scales can provide further insight into such regions of nonlinear behaviour [27].

3.3.4. Calculating the optimum bias voltage

When a purely electrical model is considered with fixed time function $C_t(t)$, it can be seen that in the steady state all electrical quantities are proportional to the voltage, so that the power given by (12) is proportional to the square of the voltage. However, when a coupled electromechanical model is considered, the voltage impacts the amplitude of the mobile mass displacement, and there is an optimal voltage which globally maximises the harvested power.

Eq. (10) is an implicit function of both a_0 and ν_t. Denoting (10) as $H(a_0, \nu_t)$ and taking the partial derivatives $H'_{a_0}(a_0, \nu_t)$ and $H'_{\nu_t}(a_0, \nu_t)$, the implicit derivative can be determined. Calculating $da_0/d\nu_t$ from $H'_{\nu_t}(a_0, \nu_t)/H'_{a_0}(a_0, \nu_t)$ and setting equal to zero, one obtains the ν_t giving maximum x. (Refer to Table 1 to scale ν_t to V_0).

$$\nu_t = \frac{-2(a_0\sigma a_1(a_0) + a_0\beta b_1(a_0))}{a_1(a_0)^2 + b_1(a_0)^2} \tag{15}$$

Both the optimum resistance and optimum bias voltage are coupled. Therefore to achieve a truly accurate representation of the optimum electrical point (R_L, V_0) both R_L and V_0 must be iterated. For this reason, the benefit of the semi-analytic methods presented in this article is that they allow an efficient calculation of variables across the parameter space, Fig. 4.

3.4. Use of MSM for optimisation of harvester design

This section uses the insight detailed in the above Sections to present an optimisation, using the multiple scales method, of the eKEH with a SGC device. It is reasonable to consider that certain parameters of the device have been previously chosen due to other constraints. The predetermined parameters for which we will optimise the system are: external vibrations (amplitude and frequency), area (S) of the device, and the parameters of the resonator (the mass, the stiffness, the damping coefficient) The external vibrations, A_{ext} and f_{ext}, are parameters that a designer cannot control. It is realistic to assume that the resonator parameters and transducer area are fixed; as for energy harvesting the mass is sought to be maximised, and in practise the device is limited by the available space. Therefore, the parameters available to a designer, include:

- The bias voltage V_0 and load resistance R_L (circuit design parameters).
- The effective transducer gap d.

The first optimisation case is presented in Fig. 4, for the experimental parameters given in Table 2, including the fixed transducer gap (d). It shows that an optimum combination of (R_L, V_0), giving the maximum power, exists. This point will shift for different external vibrations, due to the effects described in previous sections, but this circuit always presents a unique optimum solution (R_L, V_0) for sinusoidal operation.

Table 2
Parameters of the system.

Proof mass (m)	66×10^{-6} kg
No. of fingers (N)	142
Length of fingers (l)	1.97×10^{-3} m
Finger thickness (h)	380 μm
Initial gap between fingers (d_0)	43.5 μm
Aspect ratio of sidewalls (α)	0.013
Approximated gap (d) given in (20)	48.44 μm
Location of Stoppers (x_{st})	36.0 μm
Damping factor (b)	7.9×10^{-3} Ns m^{-1}
Quality factor	8.5
Spring constant (k)	68 Nm^{-1}
Area S	1.063×10^{-4} m^2

This is an important result as it shows that a global optimum exists in the electromechanical system, for the electrical parameters (R_L and V_0). This circuit is widely used to test fabricated devices, where conclusions about the performance, power yield and power density of the devices are made. Therefore to allow for a fair comparison between devices it would appear obvious that each transducer should be compared at some parameters approaching its optimum set.

The second design case presents a global optimisation to estimate the effective transducer gap corresponding to maximum power. This is achieved by calculating the optimum plane of parameters (R_L, V_0), as in Fig. 4, for multiple values of the transducer gap d. The optimum P_{max} of each plane (R_L, V_0) is plotted against its corresponding gap, presented in Fig. 5, with an external acceleration of 0.25 g.

A very important result of this simulation is an existence of an optimal value of gap maximizing the converted power. As expected, the restriction on the mass displacement reduces the maximum power, since it reduces the maximum value of the transducer capacitance over a period (C_{max}) and hence the amplitude of the charge flow generating power on the load.

The maximum convertible power is a strong function of the frequency of external vibrations. The frequency shift due to the voltage is well observed on this plot: whereas the natural resonance frequency of the mechanical resonator is 160 Hz, at 140 Hz the maximum power is more than twice greater than at 160 Hz. Indeed, since the transducer must be biased to convert power, there is an unavoidable resonance frequency shift toward lower frequencies. Note that the frequency 180 Hz is too far from the resonance, and it does not allow a significant conversion of power.

It is also advantageous that for frequencies at which there is a significant conversion of power (140 Hz and 160 Hz), the optimum gap value does not depend on the frequency. That provides a practical hint for the designer, who, therefore, can optimise the transducer device for an amplitude of external vibrations typical for its application.

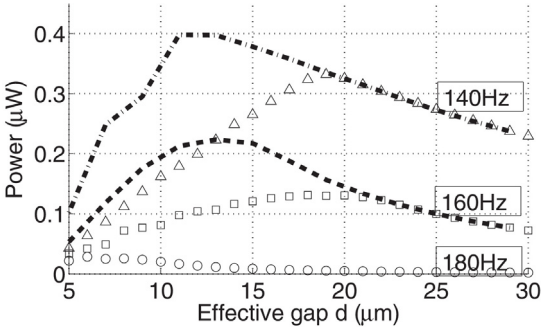

Fig. 5. Optimum power for the parameter space d, V_0 and R, for fixed external vibrations (A_{ext} = 0.25 g). Lines denote unrestricted motion (140 and 160 Hz), where 160 Hz is close to the natural resonance frequency of the unbiased mechanical resonator. The shapes detail the optimisation for the case when the mobile electrode motion is restricted to 0.75d amplitude (140, 160 and 180 Hz).

The effect on the optimum gap of limited resonator displacement is shown by shapes in Fig. 5, when mechanical stoppers restrict the motion of the oscillations to approximately 0.75 of the overall effective gap (this is the case in the practical device (Section 5.1)). This shows that in cases when the stoppers represent a significant portion of the effective gap, the 'optimal' gap can *appear* to shift. However, as shown by lines in Fig. 5, a truly optimal gap does exist. According to the particular application context and the particular design constraints, the harvested power P can be normalized by using one of the figures of merit previously proposed, e.g., the volumetric efficiency, see Eq. (13) in [28], or area/voltage normalized efficiency, see Eq. (28) in [29], and the optimization can further be carried out with use of the normalized power.

4. Coupled analysis of the system using mechanical impedance

This section presents a semi-analytical technique, based on the First Harmonic Method, which highlights design considerations of eKEH.

4.1. Mechanical impedance method

The mechanical impedance Ψ is a quantity introduced through the mathematical equivalence between the mechanical and electrical systems [21]. It is defined as $\Psi = -\dot{F}/\dot{U}$, where $\dot{F}$ is the phasor of a sinusoidal force applied to a point, and $\dot{U}$ is the phasor of the velocity of motion of this point. Note: phasor quantities are denoted with overdots, not to be confused with derivatives with respect to time. The impedance is generally defined for linear systems. However, in the case of narrow band resonators actuated by a nonlinear force whose frequency is in the resonator passband, the impedance can be written for the *fundamental* harmonic of the nonlinear force as:

$$\Psi = -\frac{\dot{F}^{\omega}}{\dot{U}}, \tag{16}$$

where $\dot{F}^{\omega}$ is the phasor of the fundamental harmonic of the force. This is only valid if the velocity of the resonator remains very close to a sinusoidal regime (the higher harmonics of the force are filtered out by the resonator character).

The work in [21] provides a detailed description of the notion of mechanical resonators for nonlinear eKEH, as well as a practical method for the calculation of the impedance of a given transducer. Two important points must be emphasized:

(1) The mechanical impedance of the electromechanical transducer depends on the transducer physics *and* on the conditioning circuit employed. Hence, the calculation of mechanical impedance requires a definition of the electrical behaviour of the conditioning electronics.
(2) The calculation of mechanical impedance is done under the assumption of a given sinusoidal motion of the mobile terminal of the transducer, with some fixed amplitude $\dot{X} = X_0 e^{j\phi_0}$ and velocity $j\omega\dot{X}$. Then, the electrical system "transducer + conditioning circuit" is simulated/analysed in the electrical domain. The resulting electrical conditions of the transducer (the voltage/current/charge evolution) define the resulting mechanical force $f_t(t)$ used for calculation of (16). The actual mechanical impedance is a function of X_0 (and not on ϕ_0).

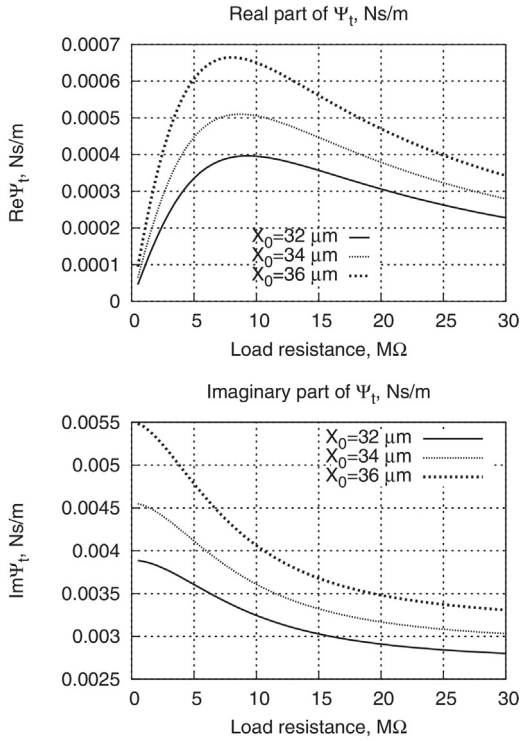

Fig. 6. Result of electrical simulations of the conditioning circuit: real and imaginary parts of the transducer impedance for different load resistances (R_L) and amplitudes of displacement (X_0), $V_0 = 10$ V, with symmetrical gap closing transducer, with parameters given in Table 2.

The mechanical impedance of the transducer Ψ_t allows a simple estimation of the power converted between the mechanical and electrical domains:

$$P = \frac{1}{2}(\omega X_0)^2 \mathrm{Re}\Psi_t, \tag{17}$$

For a transducer with a given geometry, the mechanical impedance depends on the amplitude X_0 and on the electrical parameters of the conditioning circuit. As can be seen from (3), there are only two electrical parameters: R_L and V_0. Moreover, as all electrical dynamic quantities scale with V_0, so does the transducer voltage V_t. Since f_t is proportional to V_t^2, it is enough to calculate Ψ_t for one value of $V_0 = V_{ref}$. For any other value of V_0, the transducer impedance is given by

$$\Psi_t(V_0) = \left(\frac{V_0}{V_{ref}}\right)^2 \Psi_t(V_{ref}) \tag{18}$$

Fig. 6 presents the imaginary and real parts of Ψ_t calculated for three amplitudes 32, 34, 36 μm, with $V_0 = 10$ V, and for R_L from 0.5 to 30 MΩ, for a transducer with symmetrical gap closing geometry and parameters given in Table 2, cf. discussion in Section 5.1. It can be seen that for any amplitude, there is a corresponding optimal R_L value. Also, the real part of the impedance depends strongly on the amplitude: that is explained by hyperbolic $C_t(x)$ function resulting in a strong sensitivity of C_t with regard to the vibration amplitude. It is known from the theory of electrical circuits that the imaginary part of the impedance defines the resonance frequency of the system. From Fig. 6 it can be seen that the quantity $\mathrm{Im}\Psi_t$ is a function of both V_0 and R_L. As a consequence, it is clear that not only the bias voltage affects the resonance frequency of the resonator, but also the load resistance. This is a very important result: it is often considered that the resonance frequency shift observed in resonators conditioned by a simple circuit is defined by the bias voltage. Our analysis shows that the value of the load resistance plays as important a role as V_0, and the method of mechanical impedance allows its precise calculation.

Note that the aspect of characteristics in Fig. 6 depends on the geometry of the transducer. For instance, for a non symmetrical gap-closing transducer (cf. Table 1), the imaginary part of the mechanical impedance tends to zero for very large load resistance values.

4.2. Practical use of the mechanical impedance method

Mechanical impedance method can be used straightforwardly for the analysis of the system, i.e., for the determination of the dynamics starting from the system parameters. However, such a use does not offer any advantages compared to the numerical analysis or to the above presented MSM method, since the corresponding algebraic equations are nonlinear and needs to be solved numerically.

However, the method of mechanical impedance offers a great insight into the system operation if the starting (input) information of the design is the amplitude of the mobile mass displacement, and the unknowns are some parameters of the system controlling the displacement amplitude. In this case, the mechanical impedance method solves an inverse problem, i.e., determines the parameters of the system for some desired behavior.

Here we illustrate the use of the mechanical impedance method by considering a case when the geometry of the transducer is fixed, and when it is required to chose optimal parameters of the circuit (the resistance and the voltage source) so to maximise the harvested power. In order to show the consistency of the MSM method and of the mechanical impedance method, we propose to select the displacement amplitude obtained in the first optimisation of Section 3.4, corresponding to a global maximum of the converted power (cf. Fig. 4). The amplitude is $X_0 = 20$ μm, the frequency is 150 Hz, the external acceleration is 0.25 g. The geometry of the transducer is given in Table 2. The goal of design is the selection of the parameters for the conditioning circuit which optimise the harvested power and which guarantee the wanted amplitude X_0.

According to [21], the transducer impedance Ψ_t resulting in such an amplitude is given by:

$$|\Psi_t + \Psi_r| = \frac{mA_{\mathrm{ext}}}{\omega X_0}. \tag{19}$$

where Ψ_r is the mechanical impedance of the resonator.

In order to define the two components of the complex quantity Ψ_t, an additional equation is needed. It is given by the requirement of maximisation of the converted power, expressed through Ψ_t by (17). Since the amplitude X_0 is fixed, a maximisation of the real part of the impedance is required.

We now study the mechanical impedance of the electrostatic transducer oscillating with amplitude X_0, and biased by the conditioning circuit of Fig. 1. The mechanical impedance is calculated for the desired amplitude X_0, for different sets of V_0 and R_L, the only two parameters of the electrical circuit. For the impedance calculation we use a Spice simulator which solves the electrical model presented in Section 3.1. A simple script automating the parameter variation calculates Ψ_t for all couple of values of V_0 and R_L from the grids (21, 22, 23, 24 V) and (500 kΩ, 1000 kΩ, ..., 30 MΩ). These ranges depend on the numeric values of the system parameters and, as in any approximation analysis methods, on the intuition and experience of the designer.

Now, we use the obtained $\Psi_t(R_L, V_0)$ at $X_0 = 20$ μm to choose the optimal R_L and V_0. For this, we graphically solve (19), by plotting the total mechanical impedance locus $\Psi(R_L, V_0) = \Psi_t(R_L, V_0) + \Psi_r$ on a complex plane as a family of lines, such that each line correspond to a fixed value of V_0 (Fig. 7). In this plot, the mechanical impedance of the resonator is designated by a point: it is defined for any values

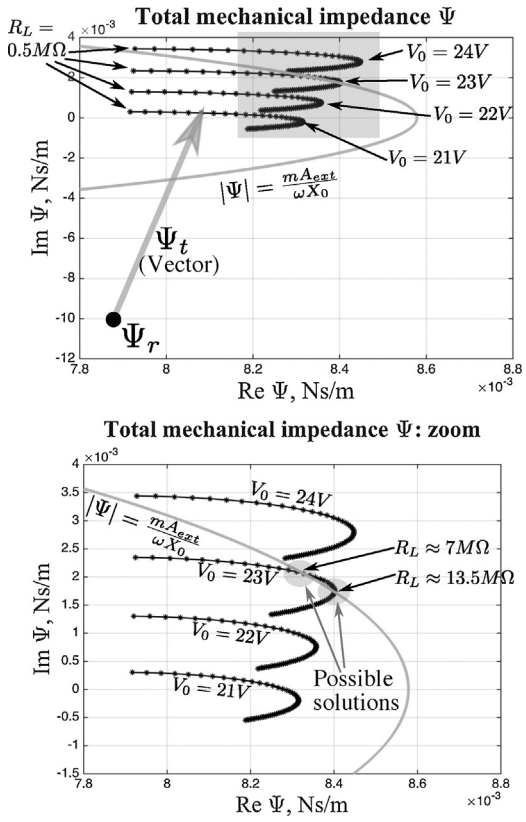

Fig. 7. The loci of the total mechanical impedance of the system $\Psi = \Psi_r + \Psi_t$ for different V_0 and R_L (black lines with stars). The grey line is the locus $|\Psi| = \frac{mA_{ext}}{\omega X_0}$. Each black line is plotted for the specified V_0 voltage, each star point in the line corresponds to a particular value of R_L. For each line, R_L varies on the grid (0.5, 1, . . ., 30) MΩ, the point with larger ImΨ correspond to the smallest load resistance.

of V_0, R_L. The grey arrow represents the vector of the transducer's impedance Ψ_t, which is added to the resonator impedance Ψ_r in order to yield the total mechanical impedance of the system.

Eq. (19) fixes the absolute value of Ψ to a constant; graphically, it means that all roots of this equation lie on the circle

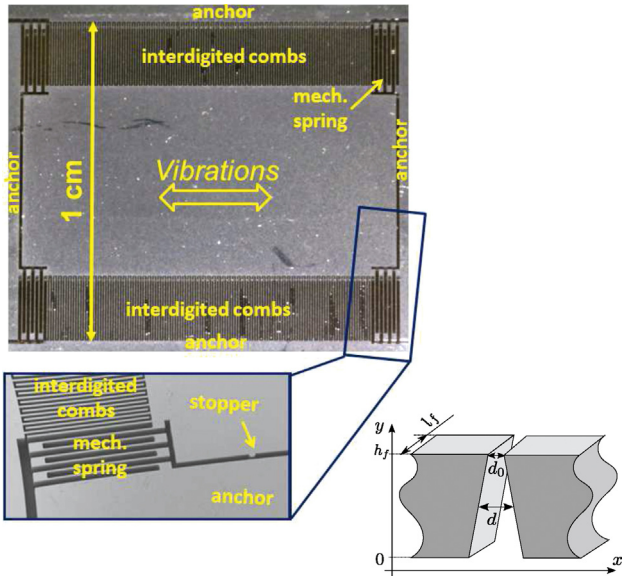

Fig. 8. Picture of the fabricated device and a diagram explaining the profile of the transducer gap.

$|\Psi| = mA_{ext}/(m\omega_{ext})$, plotted with the grey line in Fig. 7 (it looks like an oval, because of the chosen axes scale). It can be seen that several points (R_L, V_0) are roots of the equations, since the circle crosses several plots $\Psi(R_L, V_0)$.

Now, we should choose the optimal couple (R_L, V_0). We want to maximise the real part of Ψ_t. Note, that since Ψ_m is constant for a given frequency, the maximisation of $\mathrm{Re}\Psi_t$ is the same as the maximisation of $\mathrm{Re}\Psi$. Hence, in Fig. 7, we simply should chose the right most point of the grey circle crossing the impedance lines. From Fig. 7(b) (an enhanced view of Fig. 7(a)), the maximal real part of impedance corresponds to the point (13.5 MΩ, 23 V). We chose it as the solution. The corresponding value of the transducer impedance is $0.0006 + 0.0127j$ Ns m^{-1}, and according to the formula (17), with amplitude $X_0 = 20$ μm we obtain 92.4 nW for the power.

These results can be compared with Fig. 4, where the optimal power is obtained at $R_L = 13$ MΩ and $V_0 = 23.5$ V. The discrepancy in the power (the maximum power in Fig. 4 is 76.2 nW) is easily explained. The displacement amplitude, for Fig. 4, is actually $X_0 = 18.9$ μm. Therefore, using a slightly larger A_{ext} to give $X_0 = 20$ μm, the optimal MSM point is (13 MΩ, 23 V) and the power is 94 nW. Hence, the two methods produce consistent results.

What if the analysis in Section 3.4 was not done, and the amplitude of the mobile mass displacement corresponding to the maximum power is not known? In this case, we need to consider the amplitude as a parameter X_0, to use the presented algorithm for definition of a mathematical application "$X_0 \rightarrow$ *optimal power for* X_0" and optimisation X_0 for global maximisation of the power.

5. Experimental validation

5.1. Experimental device

The setup presented in this work was fabricated and tested in Université Paris-Est. It includes a silicon-based symmetrical gap-closing transducer and a continuous conditioning circuit. The parameters are shown in Table 2. A full characterisation of the device is presented in [26]. To utilize the presented analysis, a simple model of a symmetrical gap closing transducer, as shown in Table 1, was employed. To accommodate the undercut by deep reactive ion etching (DRIE), the effective gap is approximated as an average gap between the fixed and movable fingers:

$$d = d_0 + h\alpha \tag{20}$$

where h is the height of the silicon substrate and defined in the orthogonal direction to the substrate plane, α is the ratio of the silicon undercut by DRIE and d_0 is the gap between the fixed and movable fingers at the top of the comb.

To compare the theoretical values and experimental results, the maxima and minima of the capacitance C_t, were compared at a large external vibration amplitude. This allows one assume the maximum value of x as corresponding to the maximum capacitance C_{max}. The net extreme experimental values of C_t (88 pF/40 pF) compare very well with our theoretical values of 86.8 pF/38.8 pF (calculated with the formula given in Table 1, with $C_0 = \varepsilon_0 S/d$ and $x = \pm x_{st}$, other parameter values are from Table 2). This is equivalent to the method further detailed in [26].

5.2. Validation of the models with experimental results

This section presents the experimental validation of the numerical and semi-analytical (MSM) models of the harvester. The goal of the validation is to prove that the proposed models are able to predict the performances and characteristics of an implemented prototype, starting from the known prototype parameters.

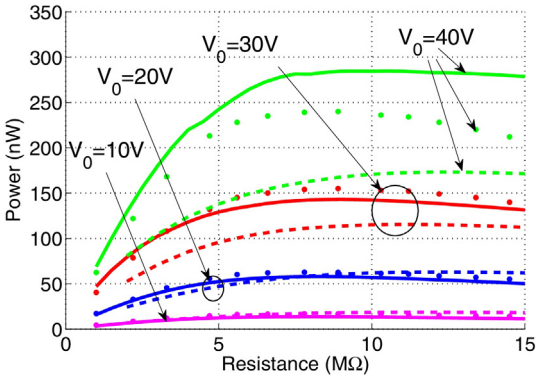

Fig. 9. Validation of the proposed models with experimental data (dots). The numerical model is shown with full lines, and the MSM model is presented by dotted lines.

Fig. 9 compares the power as a function of the load resistance (R_L), for different initial biasing voltages (V_0). Each data point was taken at the driving frequency giving the maximum power conversion. The capacitance fitting presented in Section 5.1 was made for low voltage electronics. However, high voltage (HV) electronics were required for the experiments involving electromechanical conversion, introducing a higher input parasitic capacitance (estimated to be 20 pF). Fig. 9 shows that the numerical model, (1)–(3), with added parasitic capacitance agrees very well with the experimental data with the exception of the $V_0 = 40$ V plot. This is because there are certain mechanical and electrical parameters which cannot be determined exactly, such as the lumped parameters of the device and its exact geometry. In particular, nonlinear damping, along with the shift in the resonance frequency, has a significant influence on the accuracy of the models in strong electromechanical coupling scenarios [30]. The resonator displacement amplitude is greatly affected by the bias voltage, which in turn affects the optimum load resistance. The MSM model is also in good agreement, with the exception of the strong electromechanical coupling scenarios, due to the same inaccuracies prevalent in the numerical model. The accuracy of the MSM method is further hindered by the larger shift in oscillations and omission of the parasitic capacitance. The larger bias voltage causes the dimensionless frequency term Ω to become larger and therefore reduces the accuracy of the MSM approach (which assumes all coefficients in (4a) are small).

The excitation frequency corresponding to the maximum power is presented in Fig. 10, for different biasing. From Fig. 10 the ability of both models to accurately capture the frequency shift of the maximum power due to the increasing electromechanical coupling

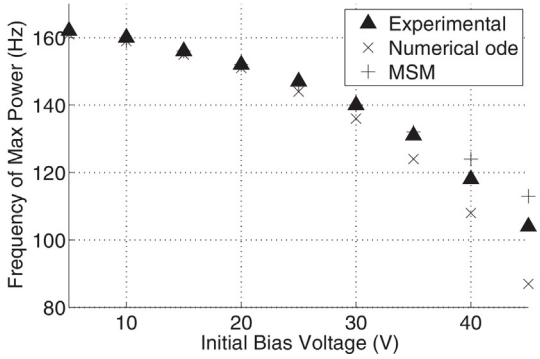

Fig. 10. Comparison of the three models showing the frequency corresponding to the maximum power for a spectrum of initial bias voltages. The resistive load R_L was fixed equal to 8.9 MΩ. The appearance of hysteresis between $V_0 = 35$ V and $V_0 = 40$ V reduces the accuracy of the models due to the increased nonlinear nature of the system.

is evident. The discrepancy in the MSM prediction of the frequency shift is under 8.6%, and the worst error is for the large voltages where, as previously mentioned, the MSM method is less precise because of the increased nonlinear behaviour. The frequency modification, due to electromechanical coupling, is given by (13).

6. Conclusion

This study presents the first consolidated study of the continuous conditioning circuit from the viewpoint of a designer. This conditioning circuit is widely used in the characterisation of electrostatic devices but very little study has focused on the circuit itself. The significant effects of the circuit configuration on the power output due to electromechanical coupling are described and explained. Both numerical and analytical analyses are presented to explain the system. The results compared well with a fabricated MEMS transducer. This article shows that, by treating the mechanical transducer and electrical circuit as one system, insights into global and transducer specific characteristics can be described. Therefore, while this circuit configuration is widely used to test transducers, analysis of the full system is required to discuss the maximal power of such a device.

The implementation of semi-analytic approaches provides a further understanding into certain phenomena which occur due to electromechanical coupling, such as: the shift in the resonance frequency, the impact of the electrical biasing on the resonator displacement and to estimate the optimal bias voltage. Using this analysis, the methods are used to optimise the system across multiple parameters. For example: a global optimum exists for the electrical parameters (R_L and V_0), to allow for a fair comparison between fabricated devices it would appear obvious that each transducer should be compared at some parameters approaching its optimum set. Both methods provide a qualitative and quantitative insight into the electromechanical action of the transducer. We believe this can be useful for a designer to understand the system operation.

Acknowledgement

This work was funded by Science Foundation Ireland.

References

[1] D. Hoffmann, B. Folkmer, Y. Manoli, Fabrication, characterization and modelling of electrostatic micro-generators, J. Micromech. Microeng. 19 (2009) 094001.
[2] E. Torres, G. Rincon-Mora, Electrostatic energy-harvesting and battery-charging CMOS system prototype, IEEE Trans. Circuits Syst. I Regul. Pap. 56 (9) (2009) 1938–1948.
[3] S.F. Bart, T.A. Lober, R.T. Howe, J.H. Lang, M.F. Schlecht, Design considerations for micromachined electric actuators, Sens. Actuators 14 (3) (1988) 269–292.
[4] K. Najafi, T. Galchev, E. Aktakka, R. Peterson, J. McCullagh, Microsystems for energy harvesting, in: 2011 16th International Solid-State Sensors, Actuators and Microsystems Conference (TRANSDUCERS), 2011, pp. 1845–1850.
[5] J. Lin, J. Zhu, M. Sonje, Y. Chang, Z. Feng, M. Almasri, Two-cavity MEMS variable capacitor for power harvesting, J. Micromech. Microeng. 22 (6) (2012) 065003.
[6] V. Janicek, M. Husak, J. Jakovenko, J. Formanek, Design and fabrication of 3D electrostatic energy harvester, Radioengineering 21 (1) (2012) 231–238.
[7] A. Fowler, S. Moheimani, S. Behrens, An omnidirectional MEMS ultrasonic energy harvester for implanted devices, J. Microelectromech. Syst. 23 (6) (2014) 1454–1462.
[8] M. Deterre, S. Risquez, B. Bouthaud, R. Dal Molin, M. Woytasik, E. Lefeuvre, Multilayer out-of-plane overlap electrostatic energy harvesting structure actuated by blood pressure for powering intra-cardiac implants, in: Journal of Physics: Conference Series, vol. 476, IOP Publishing, 2013, p. 012039.
[9] C.P. Le, E. Halvorsen, O. Sorasen, E.M. Yeatman, Microscale electrostatic energy harvester using internal impacts, J. Intell. Mater. Syst. Struct. (2012).
[10] T. Sterken, P. Fiorini, K. Baert, R. Puers, G. Borghs, An electret-based electrostatic/spl mu/-generator, in: TRANSDUCERS, 12th International Conference on Solid-State Sensors, Actuators and Microsystems, vol. 2, 2003, pp. 1291–1294.

[11] P.D. Mitcheson, T. Sterken, C. He, M. Kiziroglou, E. Yeatman, R. Puers, Electrostatic microgenerators, Meas. Control 41 (4) (2008) 114–119.
[12] Y. Suzuki, Recent progress in MEMS electret generator for energy harvesting, IEEJ Trans. Electr. Electron. Eng. 6 (2) (2011) 101–111.
[13] B. Yen, J.H. Lang, A variable-capacitance vibration-to-electric energy harvester, IEEE Trans. Circuits Syst. I Regul. Pap. 53 (2) (2006) 288–295.
[14] S. Meninger, J. Mur-Miranda, R. Amirtharajah, A. Chandrakasan, J. Lang, Vibration-to-electric energy conversion, IEEE Trans. Very Large Scale Integr. (VLSI) Syst. 9 (1) (2001) 64–76.
[15] A. de Queiroz, M. Domingues, The doubler of electricity used as battery charger, IEEE Trans. Circuits Syst. II Express Br. 58 (12) (2011) 797–801.
[16] S.G. Adams, et al., Capacitance based tunable micromechanical resonators, in: Conf. of Solid-State Sensors and Actuators, Sweden, 1995, pp. 438–441.
[17] E. Halvorsen, Energy harvesters driven by broadband random vibrations, J. Microelectromech. Syst. 17 (5) (2008) 1061–1071.
[18] F. Cottone, L. Gammaitoni, H. Vocca, Nonlinear energy harvesting, Phys. Rev. Lett. 102 (2009) 08061.
[19] S.C. Stanton, C.C. McGehee, B.P. Mann, Nonlinear dynamics for broadband energy harvesting: investigation of a bistable piezoelectric inertial generator, Phys. D Nonlin. Phenom. 239 (2010) 640–653.
[20] C.H. Nguyen, E. Halvorsen, Harmonic-balance analysis of nonlinear energy harvester models, in: 2014 IEEE International Symposium on Circuits and Systems (ISCAS), 2014, pp. 2608–2611.
[21] D. Galayko, P. Basset, A general analytical tool for the design of vibration energy harvesters (VEHs) based on the mechanical impedance concept, IEEE Trans. Circuits Syst. I Regul. Pap. 58 (2) (2011) 299–311.
[22] E. Blokhina, D. Galayko, P. Basset, O. Feely, Steady-state oscillations in resonant electrostatic vibration energy harvesters, IEEE Trans. Circuits Syst. I Regul. Pap. 60 (4) (2013) 875–884.
[23] D. Galayko, E. Blokhina, P. Basset, F. Cottone, A. Dudka, E. O'Riordan, O. Feely, Tools for analytical and numerical analysis of electrostatic vibration energy harvesters: application to a continuous mode conditioning circuit, in: Journal of Physics: Conference Series, vol. 476, IOP Publishing, 2013, p. 012076.
[24] A.H. Nayfeh, D.T. Mook, Nonlinear Oscillations, John Wiley & Sons, 2008.
[25] E. Kreyszig, Advanced Engineering Mathematics, Wiley, New York, 1999.
[26] P. Basset, D. Galayko, F. Cottone, R. Guillemet, E. Blokhina, F. Marty, T. Bourouina, Electrostatic vibration energy harvester with combined effect of electrical nonlinearities and mechanical impact, J. Micromech. Microeng. 24 (3) (2014) 035001.
[27] E. O'Riordan, A. Dudka, D. Galayko, P. Basset, O. Feely, E. Blokhina, Capacitive energy conversion with circuits implementing a rectangular charge-voltage cycle. Part 2: Electromechanical and nonlinear analysis, IEEE Trans. Circuits Syst. I Regul. Pap. 62 (11) (2015) 2664–2673.
[28] P. Mitcheson, E. Yeatman, G. Rao, A. Holmes, T. Green, Energy harvesting from human and machine motion for wireless electronic devices, Proc. IEEE 96 (9) (2008) 1457–1486.
[29] P. Basset, D. Galayko, A. Mahmood Paracha, F. Marty, A. Dudka, T. Bourouina, A batch-fabricated and electret-free silicon electrostatic vibration energy harvester, J. Micromech. Microengin. 19 (2009) 115025.
[30] T. Veijola, H. Kuisma, J. Lahdenper, T. Ryhnen, Equivalent-circuit model of the squeezed gas film in a silicon accelerometer, Sens. Actuators A Phys. 48 (3) (1995) 239–248.

Biographies

Eoghan O'Riordan received a B.E. in electrical engineering from University College Dublin in 2012. He is currently working toward a Ph.D. degree in electronic engineering at UCD. His research interests include nonlinear dynamics, and vibration energy harvesting.

Dimitri Galayko graduated from Odessa State Polytechnich University (Ukraine) in 1998, received his masters degree from INSA-LYON, France in 1999, and obtained his PhD degree from the University Lille-I in 2002. Since 2005 he is an associate professor in UPMC in the LIP6 laboratory. His research interests include study, modeling and design of nonlinear integrated circuits for sensor interface and mixed-signal applications.

Philippe Basset received his M.Sc. and Ph.D. from IEMN University of Lille in 1999 and 2003, respectively. His research interests include micro/nano-structuration of silicon and micropower sources for autonomous MEMS. He led several projects on energy harvesting using micro- and nano-technologies and he serves on the PowerMEMS conference TPC since 2013.

Elena Blokhina received the M.Sc. and Ph.D. degrees in physics from Saratov State University, Saratov, Russia, in 2002 and 2005, respectively. Since 2007, she has been with University College Dublin, Ireland, where she currently is a lecturer. Her research interests include nonlinear dynamics and oscillation theory and their application to the analysis of MEMS and energy harvesters. Dr. Blokhina is a Senior IEEE member and is a member of the IEEE Technical Committee on Nonlinear Circuits and Systems.